Korean J. Chem. Eng., **31**(8), 1384-1388 (2014)
DOI: 10.1007/s11814-014-0037-z

pISSN: 0256-1115
eISSN: 1975-7220

Effect of membrane-electrode-assembly configuration on proton exchange membrane fuel cell performance

Sehkyu Park*,,† and Branko N. Popov***

*Center for Electrochemical Engineering, Department of Chemical Engineering, University of South Carolina, Columbia, SC 29208, USA
**Department of Chemical Engineering, Kwangwoon University, Seoul 139-701, Korea
(*Received 7 November 2013 • accepted 28 January 2014*)

Abstract−Four different membrane-electrode-assemblies (MEAs) with single and dual-layer gas diffusion layers (GDLs) at the anode and the cathode were prepared to examine polarization characteristics that rely on MEA configuration. Porous structure of single and dual-layer GDLs was investigated using a mercury porosimeter. An MEA with dual-layer GDLs at each electrode demonstrated higher performance with an air feed. To comprehend the improvement, the impedance behavior at various current densities and polarization behavior under back pressure were analyzed in terms of oxygen diffusion processes that control catalyst utilization in the gas diffusion electrode.

Keywords: Proton Exchange Membrane Fuel Cells, MEA Configuration, Gas Diffusion Layer, Microporous Layer, Water Management

INTRODUCTION

A gas diffusion layer (GDL) in PEM fuel cells is a key component to enhance fuel and oxidant diffusion, provide electron pathway, act as a physical support under compression, and control water flow in the MEA to determine an effective three phase boundary in the catalyst layer (CL) where electrochemical reactions primarily take place. There are two types of GDLs for PEM fuel cell applications: single-layer GDLs of a carbon-based macroporous substrate (MPS) such as carbon paper and carbon cloth and dual-layer GDLs made up of a carbon-based MPS and microporous layer (MPL) that contains carbon powder and hydrophobic polymer [1-4].

Numerous theoretical and experimental works on a dual-layer GDL have been conducted by many fuel cell scientists and engineers who generally propose capillary-driven flow as a primary mechanism for the water transport, in terms of cathode MPL properties affected by carbon type, carbon loading (or MPL thickness), hydrophobic polymer content, etc [4-13]. Their results have demonstrated that the MPL at the cathode adjusts capillary pressure of liquid water and its back diffusion through the membrane, thus tailoring water saturation level in the CL and the MPS at the cathode. On the other hand, hydrophilic cathode MPLs were also introduced by several research groups who primarily claim that liquid water transport through hydrophilic channels by wicking effect and water vapor formed in the CL moves towards the gas flow channel with phase change in the presence of temperature difference (i.e., phase-change induced flow) [14-19]. Yet, if it can be assumed that the temperature gradient across a multi-layered structure in PEM fuel cells is considerably small, it is easily accepted that capillary action in the hydrophobic channels at the cathode is the dominant process for the water removal. As a result, a dual-layer GDL has been mostly applied to the cathode compartment, based on capillary-driven flow mechanism. However, a subject that covers different MEA configurations at the anode (e.g., embedment of anode MPL at the anode) garners less attention and is not extensively considered because of the relatively low water saturation and high fuel concentration at the anode.

In this study, the MEAs with four different configurations, illustrated in Fig. 1, were prepared: i) catalyst-coated membrane (CCM) with two MPS on both sides (MEA1 or No MPL), ii) CCM with a dual-layer GDL at the anode and an MPS at the cathode (MEA2 or AMPL), iii) CCM with an MPS at the anode and a dual-layer GDL at the cathode (MEA3 or CMPL), and iv) CCM with two dual-

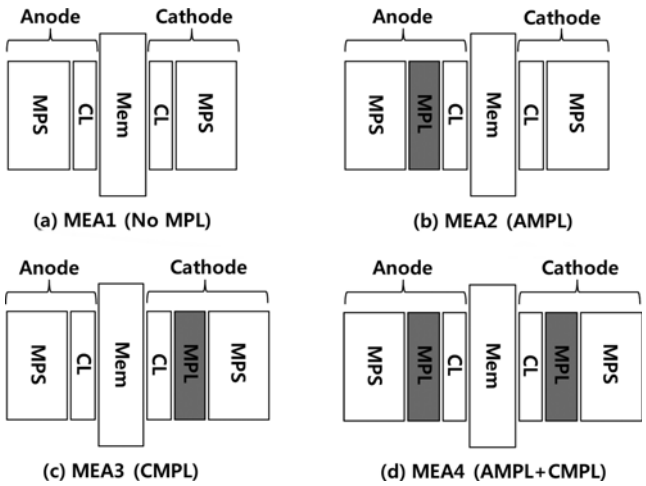

Fig. 1. Four different configurations of MEAs.
(a) MEA with no MPL at the anode and the cathode (MEA1 or no MPL), (b) MEA with anode MPL (MEA2 or AMPL), (c) MEA with cathode MPL (MEA3 or CMPL), and (d) MEA with anode MPL and cathode MPL (MEA4 or AMPL+CMPL)

†To whom correspondence should be addressed.
E-mail: vitalspark@kw.ac.kr

layer GDLs on both sides (MEA4 or AMPL+CMPL). Porous structure of single and dual-layer GDL, and electrochemical properties such as polarization behavior and impedance responses of the MEAs were investigated to understand the effect of MEA configuration on reactant diffusion and water management in PEM fuel cells.

EXPERIMENTAL

1. Preparation of Microporous Layer on the Carbon Paper

A carbon slurry for the MPL was prepared by mixing carbon powders (acetylene black) with isopropanol, glycerol, and PTFE-dispersed water (60 wt% PTFE, Alfa Aesar) in an ultrasonic bath for 2 h. The carbon slurry was blade-coated onto one side of carbon paper treated with 10 wt% PTFE (SGL 10CA, SGL Carbon Group) and pressed between two rotating drums at 80 °C. An MPL-coated carbon paper was heat-treated at 280 °C for 30 min to remove glycerol within the pores of the MPL, and then at 350 °C for 30 min to distribute PTFE throughout the MPL. In the MPL, the carbon loading and the PTFE content were fixed to be 2.0 mg cm^{-2} and 20 wt%, respectively [20].

2. Preparation Of Membrane-electrode Assembly

A catalyst ink was prepared by ultrasonically blending Pt/C powders (45 wt% Pt, Tanaka) with Nafion solution (5 wt% Nafion, Alfa Aesar), deionized water and methanol for 2 h. The catalyst ink was sprayed onto both sides of the Nafion 112 membrane, followed by drying at 80 °C for 2 min. Pt loading on each side of the membrane was made to be 0.4 mg cm^{-2}. Then, the GDLs of interest were placed on each catalyst layer.

3. Physical and Electrochemical Characterization

Pore structure of the GDL with and without MPL was examined by using a mercury porosimeter (Micromeritics Autopore 9400). Pore size distribution (PSD) of the GDL was obtained from the mercury intrusion data (i.e., the volume of mercury filling the pores as a function of the pressure).

Electrochemical measurements were performed in a single cell with serpentine flow channels. Hydrogen humidified at 77 °C and air humidified at 75 °C were introduced to the anode and cathode compartments, respectively. All the measurements were at 75 °C and at ambient pressure. The hydrogen stoichiometry λ_{H2} and air stoichiometry λ_{air} during fuel cell operation were 1.2 and 2.0, respectively, and the geometric area of the MEA used in this study was 25 cm^2. The electrochemical impedance spectroscopy (EIS) was carried out at different current densities from 0 to 0.8 A cm^{-2} over the frequency range from 10 mHz to 10 kHz. The EIS measurement was performed at constant flow rate (i.e., ν_{H2}=500 cm^3 min^{-1} and ν_{air}=1,000 cm^3 min^{-1}).

RESULTS AND DISCUSSION

During the preparation of four different MEAs in Fig. 1, the catalyst ink was directly coated onto both sides of the membrane to avoid modification of the GDL structure and ensure a well-defined interface between the catalyst layer (CL) and the GDL. The interface of MPL/MPS is quite different from that between CL and GDL since the MPS is incorporated with the MPL during the preparation. Hence, it is of great importance to observe porous structure of bare GDL and dual-layer GDL.

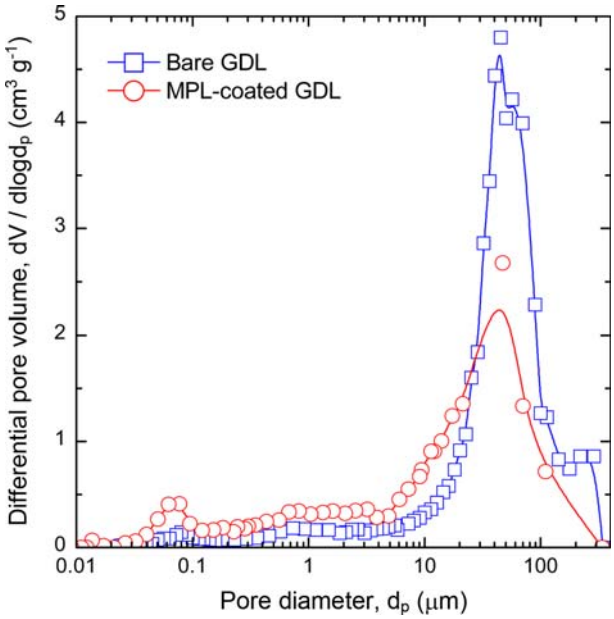

Fig. 2. PSD curves (dV/dlogd$_p$) for the GDLs with and without MPL.

PSD curves for bare GDL and MPL-coated MPS are illustrated in Fig. 2. For bare GDL, a hump followed by the main peak of PSD appears between 20 and 300 μm, and then a relatively small volume of pores less than 10 μm is observed, which indicates the bare GDL surface contains macropores between 150-300 μm (i.e., first hump) and carbon fibers mingled with thermoset resin mostly makes void space of 20-100 μm (i.e., main peak). On the other hand, a broad peak between 5-150 mm and a narrow peak at 0.05-0.1 μm are found for the MPL-coated MPS. This means the carbon slurry has partly intruded into the macropores (>40 μm) in the MPS, forming a dual PSD with more mesopores at 0.1-5 μm. In addition, no complete

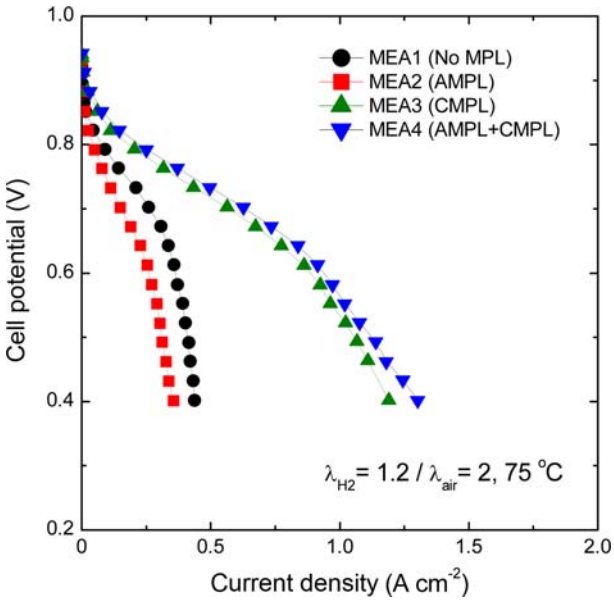

Fig. 3. Polarization curves of the MEAs with different configurations. The experiments were performed under the constant stoichiometry mode of λ_{H2}=1.2 and λ_{air}=2.0.

penetration of carbon slurry through the MPS is observed during the preparation of the dual-layer GDL. It is thus inferred from the PSD data that macropores primarily reside at the channel side of the MPS, mesopores on the other side of the MPS and micropores form near the interface between the MPL and the MPS.

Fig. 3 presents polarization curves of the PEM fuel cells measured by using four different MEA configurations. As clearly seen in Fig. 3, MEA1 (or No MPL) and MEA2 (or AMPL) show appreciably poor polarization behavior, which is presumably due to severe water accumulation at the cathode MPS. The capillary pressure in a hydrophobic diffusion medium can be expressed as [21]:

$$p_c = \frac{\sigma \cos\theta_c}{(K_{abs}/\varepsilon)^{1/2}}(1.417s - 2.120s^2 + 1.263s^3) \quad (1)$$

with

$$\frac{K_{abs}}{\varepsilon} = \frac{d_{p,avg}^2}{16} \quad (2)$$

Where s, θ_c, s, K_{abs}, ε, $d_{p,avg}$, denote the surface tension of liquid water, the contact angle of liquid water on the solid surface, the liquid water saturation, the absolute permeability, the bulk porosity, and the average pore diameter in a diffusion medium, respectively. Since capillary pressure is identical at the interface, there exists a sudden leap of liquid water saturation at the interface between the CL and the MPS with $\theta_{c,CL}>90^o$ (i.e., $s_{CL}<s_{MPS}$ at the interface of CL/MPS) [10]. However, the water transferred from the anode and produced at the cathode mostly dwells within the pores of the cathode MPS because of much larger pores in the MPS by several orders of magnitude (as expected from Fig. 2) than those in the CL. This results in considerably low capillary pressure (i.e., $p_c \propto 1/d_{p,avg}$), thus impeding oxygen diffusion toward catalytic active sites through the MPS [22]. In addition, a poorer performance of MEA2 (or AMPL) is also observed in Fig. 3. It is surmised that the anode MPL blocks water back diffusion from the cathode to the anode through the membrane as the water is accumulated in the CL at the anode, resulting in more severe water saturation in the cathode MPS.

In Fig. 3, conversely, the presence of cathode MPL significantly enhanced fuel cell performance when air was used as an oxidant. This polarization behavior is in qualitatively good agreement with the results obtained from many research groups [4-13,23,24]. They claim that the cathode MPL increases capillary pressure, which pushes the water away toward the gas flow channel and/or facilitates water transport to the anode through the membrane. More interestingly, the cathode MPL in combination with the anode MPL in this study displays a more beneficial effect in polarization characteristics. To further examine how the MEA with both anode MPL and cathode MPL affects fuel cell performance, EIS experiments that could characterize electrochemical and diffusion processes with different relaxation time were carried out.

Fig. 4 depicts charge transfer resistance R_{ct} at various current densities for MEA3 (or CMPL) and MEA4 (or AMPL+CMPL). R_{ct} for both MEA3 (or CMPL) and MEA4 (or AMPL+CMPL) decreases as current density increases, but it increases in the high current densities (>0.4 A cm^{-2}). This tendency of R_{ct} is believed to be strongly associated with the dependence of ORR kinetics on oxygen diffusion across the cathode. This may be explained by thin film-flooded agglomerate dynamics of gas diffusion electrodes consisting of cylindrical macropores and porous agglomerate region covered by thin electrolyte film [25,26]. According to these dynamics, the oxygen with no concentration gradient along the macropore radially diffuses towards the porous agglomerate region made up of carbon-supported Pt catalyst intermixed with the ionomer (i.e., agglomerate diffusion) through a thin ionomer film (i.e., thin film diffusion). Such oxygen diffusion is dependent on the cell potential that influences effective porosity of the cathode gas diffusion electrode relevant to water formation. So at small cathode overpotentials (or small current densities), R_{ct} is reduced because of its dependency on agglomerate diffusion, while it grows due to thin film diffusion limitation at high cathode overpotentials (or high current densities). In a macroscopic view, porous agglomerate regions and thin electrolyte films have been interpreted as CL and non-CL including MPL and MPS respectively, and two representative oxygen diffusion processes have been assumed to be governed by water saturation level across the cathode, depending on cathode overpotential (or current density) [27,28]. In terms of the two oxygen diffusion processes introduced, the results from EIS experiment imply ORR kinetics at low current densities (<0.4 A cm^{-2}) is primarily affected by oxygen diffusion in the CL, while at high current densities (>0.4 A cm^{-2}) mass transport limitation occurs at the GDL, resulting in slow electrochemical processes in the CL. More importantly, as given in Fig. 4, all values of R_{ct} for MEA4 (or AMPL+CMPL) are smaller than R_{ct} for MEA3 (or CMPL), indicating MEA4 (or AMPL+CMPL) provides a lower oxygen concentration gradient through the CL and the GDL due to lower water saturation level across the MEA over the whole range of current densities. It is postulated that for MEA4 (or AMPL+CMPL), more water is accumulated in the anode CL in the presence of anode MPL, which results in i) the loss of available catalytic active sites in the anode CL, ii) the formation of relatively high threshold pressure that could further push water away towards the anode gas flow channel, iii) feasibly better hydration of the mem-

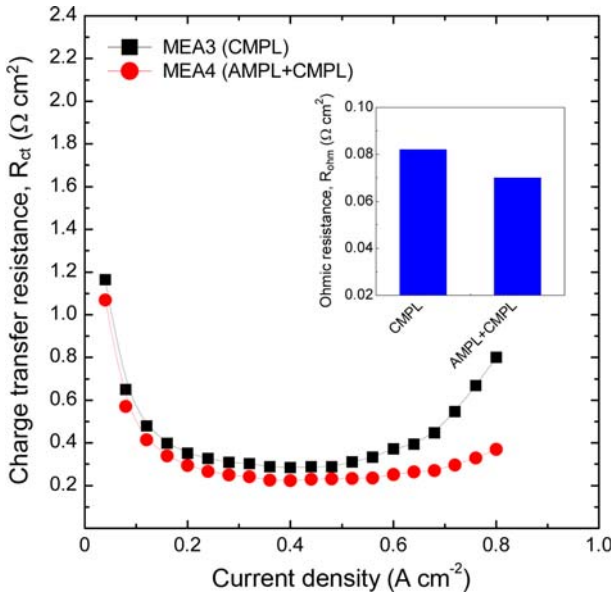

Fig. 4. AC-impedance spectra of the MEAs with cathode MPL only and both anode and cathode MPL as a function of current density. (Inset) ohmic resistance obtained from *x*-intercept in Nyquist plot.

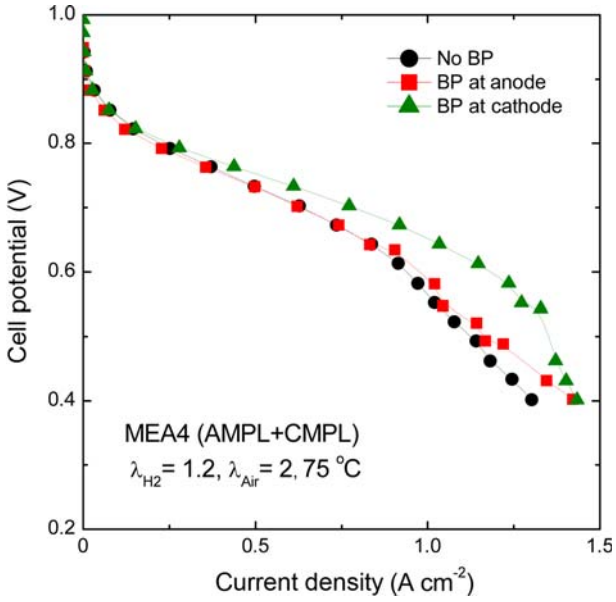

Fig. 5. Polarization curves of the MEA with anode and cathode MPL under different back pressures.

brane leading to an improvement in proton conductivity inversely proportional to membrane resistance (see the inset), and iv) relatively high capillary pressure between the cathode CL and MPL to force water out because of reduced water concentration gradient across the membrane.

To obtain a better understanding of the mass transport in MEA4 (or AMPL+CMPL), polarization curves of MEA4 (or AMPL+CMPL) with different back pressures were plotted in Fig. 5. It is generally attributed to an increased reactant partial pressure that reduces hydrogen or oxygen concentration gradient at the anode and the cathode, respectively, thereby enhancing fuel cell performance. In this study, as compared to the MEA with no back pressure, the MEA with back pressure at the anode reveals a better polarization behavior at the concentration-controlled region (>0.9 A cm^{-2}), while for the MEA with back pressure at the cathode a higher performance is observed at intermediate and high current densities (>0.3 A cm^{-2}) where it is believed oxygen diffusion limitation takes place in the CL and the GDL, respectively [29]. It stands to reason from the above results that the polarization characteristics are dependent on water management both in the CL and the GDL at the cathode [28], and water saturation in the GDL (rather than the CL) at the anode. It can be concluded from experimental polarization curves and EIS data that the performance improvement of the MEA with anode MPL and cathode MPL (MEA4) is attributed to enhanced oxygen diffusion in the cathode CL and GDL and the anode GDL due to effective water management achieved by both cathode MPL and anode MPL, and ohmic benefit of the membrane at the expense of relatively high saturation in the anode CL.

CONCLUSIONS

MEAs with different MEA configurations were fabricated and characterized using mercury porosimetry, polarization technique, and electrochemical impedance spectroscopy (EIS). The MEA with anode and cathode MPL demonstrated higher performance than the MEA with no MPL, anode MPL, or cathode MPL. It is suggested that the MEA with a combination of cathode MPL and anode MPL facilitates water management in both the CL and the GDL at the cathode and in the GDL at the anode, thus enhancing fuel and oxidant diffusion toward catalytic active sites.

ACKNOWLEDGEMENTS

Financial support provided by FUJIFILM Manufacturing U.S.A., Inc. is acknowledged gratefully. The present work was also supported by the Research Grant of Kwangwoon University in 2013.

REFERENCES

1. M. Mathias, J. Roth, J. Fleming and W. Lehnert, *in Handbook of fuel cells*, W. Vielstich, A. Lamm and H. A. Gasteiger Eds., John Wiley & Sons, New York (2003).
2. F. Barbir, *PEM fuel cells*, Elsevier Academic Press, Burlington (2005).
3. M. V. Williams, E. Begg, L. Bonville, H. R. Kunz and J. M. Fenton, *J. Electrochem. Soc*., **151**, A1173 (2004).
4. S. Park, J. W. Lee and B. N. Popov, *Int. J. Hydrog. Energy*, **37**, 5850 (2012).
5. V. A. Paganin, E. A. Ticianelli and E. R. Gonzalez, *J. Appl. Electrochem*., **26**, 297 (1996).
6. F. Lufrano, E. Passalacqua, G. Squadrito, A. Patti and L. Giorgi, *J. Appl. Electrochem*., **29**, 445 (1999).
7. E. Passalacqua, G. Squadrito, F. Lufrano, A. Patti and L. Giorgi, *J. Appl. Electrochem*., **31**, 449 (2001).
8. Z. Qi and A. Kaufman, *J. Power Sources*, **109**, 38 (2002).
9. E. Antolini, R. R. Passos and E. A. Ticianelli, *J. Power Sources*, **109**, 477 (2002).
10. J. H. Nam and M. Kaviany, *Int. J. Heat Mass Transfer*, **46**, 4595 (2003).
11. U. Pasaogullari and C. Y. Wang, *Electrochim. Acta*, **49**, 4359 (2004).
12. G. G. Park, Y. J. Sohn, T. H. Yang, Y. G. Yoon, W. Y. Lee and C. S. Kim, *J. Power Sources*, **131**, 182 (2004).
13. A. Z. Weber and J. Newman, *J. Electrochem. Soc*., **152**, A677 (2005).
14. S. Park, J. W. Lee and B. N. Popov, *J. Power Sources*, **177**, 457 (2008).
15. A. Z. Weber and J. Newman, *J. Electrochem. Soc*., **153**, A2205 (2006).
16. S. Kim and M. M. Mench, *J. Electrochem. Soc*., **156**, B353 (2009).
17. L. Cindrella, A. M. Kannan, R. Ahmad and M. Thommes, *Int. J. Hydrog. Energy*, **34**, 6377 (2009).
18. Y. X. Wang, S. Al Shakhshir and X. G. Li, *Appl. Energy*, **88**, 2168 (2011).
19. R. Schweiss, M. Steeb and P. M. Wilde, *Fuel Cells*, **10**, 1176 (2010).
20. M. Ahn, Y. H. Cho, J. Kim, N. Jung and Y. E. Sung, *Electrochim. Acta*, **56**, 2450 (2011).
21. M. Kaviany, *Principles of heat transfer in porous media*, Springer-Verlag, New York (1991).
22. S. Park and B. N. Popov, *Electrochim. Acta*, **54**, 3473 (2009).
23. C. S. Kong, D. Y. Kim, H. K. Lee, Y. G. Shul and T. H. Lee, *J. Power Sources*, **108**, 185 (2002).

24. G. Lin and T. V. Nguyen, *J. Electrochem. Soc*., **152**, A1942 (2005).
25. T. E. Springer and I. D. Raistrick, *J. Electrochem. Soc*., **136**, 1594 (1989).
26. I. D. Raistrick, *Electrochim. Acta*, **35**, 1579 (1990).
27. M. Ciureanu and R. Roberge, *J. Phys. Chem. B*, **105**, 3531 (2001).
28. Y. Bultel, K. Wiezell, F. Jaouen, P. Ozil and G. Lindbergh, *Electrochim. Acta*, **51**, 474 (2005).
29. T. E. Springer, M. S. Wilson and S. Gottesfeld, *J. Electrochem. Soc*., **135**, 1594 (1989).